

Charmless decays  $B \rightarrow \pi, K$  and  $K\bar{K}$  in broken  $SU(3)$  symmetry

Yue-Liang Wu

Institute of Theoretical Physics, CAS, Beijing, 100080, China

Yu-Feng Zhou

Institute for Physics, Dortmund University, D-44221, Dortmund, Germany<sup>y</sup>

## Abstract

Charmless  $B$  decay modes  $B \rightarrow \pi, K$  and  $K\bar{K}$  are systematically investigated with and without favor  $SU(3)$  symmetry. Independent analyses on  $\pi$  and  $K$  modes both favor a large ratio between color-suppressed tree (C) and tree (T) diagram, which suggests that they are more likely to originate from long distance effects. The sizes of QCD penguin diagrams extracted individually from  $\pi, K$  and  $K\bar{K}$  modes are found to follow a pattern of  $SU(3)$  breaking in agreement with the naive factorization estimates. Global fits to these modes are done under various scenarios of  $SU(3)$  relations. The results show good determinations of weak phase  $\gamma$  in consistency with the Standard Model (SM), but a large electro-weak penguin ( $P_{EW}$ ) relative to  $T + C$  with a large relative strong phase are favored, which requires an big enhancement of color suppressed electro-weak penguin ( $P_{EW}^C$ ) compatible in size but destructively interfering with  $P_{EW}$  within the SM, or implies new physics. Possibility of sizable contributions from nonfactorizable diagrams such as  $W$ -exchange (E), annihilation (A) and penguin-annihilation diagrams ( $P_A$ ) are investigated. The implications to the branching ratios and CP violations in  $K\bar{K}$  modes are discussed.

PACS numbers: 13.25.Hw, 11.30.Er, 11.30.Hv

---

 Email: ylwu@itp.ac.cn

<sup>y</sup>Email: zhou@zybn.physik.uni-dortmund.de

## I. INTRODUCTION

In the recent years, the two  $B$ -factories have succeed in steadily improving the measurements of hadronic charmless  $B$  decays. At present, all the branching ratios of  $B \rightarrow K$  modes have been measured with good accuracy. The large direct CP violations have also been established in  $B \rightarrow K$  and  $B \rightarrow K^*$  modes [1]. Their implications have been reported in a recent short paper [2]. It has been shown that the weak phase  $\alpha$  can well be determined to be consistent with the standard model, it prefers a relative large electroweak penguin with a large strong phase and also favors an enhanced color-suppressed tree diagram. In this longer paper, we shall provide a more detailed analysis with including subleading diagrams and their implications to  $B \rightarrow K$  modes as well as paying attention to SU(3) broken effects.

It is of interest to note that the signs of the direct CP violations, if confirmed by the future experiments would agree with the results from perturbative QCD approach [3, 4] while pose a challenge to the naive factorization [5, 6] and QCD factorization calculations [7, 8, 9, 10]. These impressive new results have triggered a large amount of theoretical efforts to understand the strong interaction dynamics of those decays [11, 12, 13, 14, 15], extract the weak phases in the Cabibbo-Kobayashi-Maskawa (CKM) matrix [16, 17] and explore new physics [18, 19, 20, 21, 22, 23, 24].

Making use of the flavor topology of the decay amplitudes and the approximate flavor SU(3) symmetry, one can describe those decay modes in terms of several independent quark flavor diagrams, such as tree diagram (T), color-suppressed tree diagram (C), QCD penguin diagram (P), electroweak penguin diagram ( $P_{EW}$ ) and color suppressed electroweak penguin diagram ( $P_{EW}^C$ ) etc. It then follows from the hierarchies of the Wilson coefficients and the CKM matrix elements that the  $B \rightarrow K$  modes are T dominant while  $B \rightarrow K^*$  modes are P dominant. Since C is color suppressed, one expects that the hierarchical structures among those decays should be

$$2\text{Br}(B \rightarrow K^0) \sim \text{Br}(B \rightarrow K^*) \sim 2\text{Br}(B \rightarrow K^0); \quad (1)$$

and

$$\text{Br}(B \rightarrow K^*)' \sim \text{Br}(B \rightarrow K^0)' \sim 2\text{Br}(B \rightarrow K^0)' \sim 2\text{Br}(B \rightarrow K^0); \quad (2)$$

respectively.

Note that the above relations follow from a purely short distance diagrammatic description which could be misleading in the presence of large final state interactions (FSIs) [25, 26, 27]. At present, they are not favored by the experiments. The current data listed in Tab.I, show big enhancements of  $\text{Br}(B \rightarrow K^0)$  and  $\text{Br}(B \rightarrow K^0)$  relative to  $\text{Br}(B \rightarrow K^*)$  and suppression of  $\text{Br}(B \rightarrow K^*)$  relative to  $2\text{Br}(B \rightarrow K^0)$  and  $\text{Br}(B \rightarrow K^0)$ . The numerical values of these relative ratios are given by [20]

$$\begin{aligned} R_+ &= 2 \frac{\text{Br}(B \rightarrow K^0)}{\text{Br}(B \rightarrow K^*)} \frac{\text{Br}_{B^0}}{\text{Br}_{B^+}} = 2.2 \pm 0.31; \\ R_{00} &= 2 \frac{\text{Br}(B \rightarrow K^0)}{\text{Br}(B \rightarrow K^*)} = 0.67 \pm 0.14; \end{aligned} \quad (3)$$

m odes	Br( 10 <sup>-6</sup> )	a <sub>CP</sub>	S
<sup>+</sup>	4:6 0:4	0:37 0:11	0:61 0:14
<sup>0 0</sup>	1:51 0:28	0:28 0:39	
<sup>0</sup>	5:5 0:6	0:02 0:07	
<sup>+</sup> K	18:2 0:8	0:11 0:02	
<sup>0</sup> K <sup>0</sup> (K <sub>S</sub> )	11:5 1:0	0:09 0:14	( 0:34 0:28)
<sup>0</sup> K	24:1 1:3	0:02 0:034	
<sup>0</sup> K	12:1 0:8	0:04 0:04	
K <sup>+</sup> K			
K <sup>0</sup> K <sup>0</sup>	1:19 <sup>+0:42</sup> <sub>0:37</sub>		
K <sup>0</sup> K <sup>0</sup>	< 2:4 (1:45 <sup>+0:53</sup> <sub>0:46</sub> )		

TABLE I: The latest world averaged data of Charm less B decays[28].

and also

$$\begin{aligned}
R_n &= \frac{\text{Br}(\text{}^+K)}{2\text{Br}(\text{}^0K^0)} = 0:79 \quad 0:08; \\
R &= \frac{\text{Br}(\text{}^+K)}{\text{Br}(\text{}^0K^0)} \frac{B^+}{B^0} = 0:82 \quad 0:06; \\
R_2 &= \frac{\text{Br}(\text{}^+K)}{2\text{Br}(\text{}^0K^0)} \frac{B^+}{B^0} = 0:81 \quad 0:06; \tag{4}
\end{aligned}$$

The above ve ratios characterize the puzzling patterns of the latest data and may provide insights on the strong dynamics of heavy quark decays or possible new physics beyond the Standard Model (SM).

The large value of  $R_{00}$  forces the  $C$  to be large, which is a challenge to theory. Various ways to explain large  $R_{00}$  with reasonable values of  $C=T$  involve an enhanced  $W$ -exchange diagram (E), a large QCD penguin contribution corresponds to  $u$ -quark loop or large  $n$ al state interactions (FSIs) which involves  $DD_{(s)}$  intermediate states and quasi-elastic mixing between  $^+$  and  $^0 0$  modes [14]. Note that the and  $K$  modes differ in favor topological structure while FSIs are favor blind, the two kind of effects can in principle be distinguished by a separated study of these two sets. FSI will lead to large  $C$  in all decays modes. Furthermore, it should enhance  $P_{EW}^C$  relative to  $P_{EW}$  in a similar manner.

In the  $K$  modes, it is well known that the suppression of  $R_n$  is more relevant to the electro-weak penguin sector, as in  $K$  modes  $T$  and  $C$  are greatly suppressed by small CKM matrix elements, In the SM, from the isospin structure of the effective Hamiltonian, the ratio between electroweak penguin and tree diagrams are fixed through [29, 30, 31, 32, 33]

$$R_{EW}^{SM} = \frac{P_{EW} + P_{EW}^C}{T + C} = \frac{3}{2} \frac{C_9 + C_{10}}{C_1 + C_2} = (1:35 \quad 0:12) \quad 10^2; \tag{5}$$

for modes. Where  $T, C, P_{EW}$  and  $P_{EW}^C$  are diagrams with CKM matrix elements factorized out which will be discussed in detail below.  $C_i$ s stand for the short distance Wilson coefficients at the scale of  $\mu = m_b$ . This relation is free from hadronic uncertainties

and survives under elastic FSIs and inelastic FSIs through low isospin states such as  $B \rightarrow D_s^* \pi^0$  ( $K$ ). It also predicts the direct CP violation in  $B \rightarrow D_s^* \pi^0$  modes to be vanishing. Using flavor SU(3) symmetry, this relation also holds for  $K$  modes. Thus it can directly confront the experiments and allows us to explore the new physics in hadronic charmless B decays. It is of interest that the charmless B decay data indeed imply the violation of Eq.(5). The possibility of larger isospin  $I = 2(3=2)$  amplitudes violating Eq.(5) in  $B \rightarrow D_s^* \pi^0$  ( $K$ ) modes was found in Ref.[34] and recently discussed in Refs.[2, 18, 19, 20, 35, 36, 37, 38] with updated data. In a recent analysis, an enhancement of a factor of two was obtained through a direct global  $\chi^2$  analysis using flavor SU(3) symmetry [2].

Although it is too early to draw any robust conclusion, it motivates us to take a closer look at the electroweak penguin sector within and beyond the SM. Note that in these analyses on large  $P_{EW}$ , the effects of  $P_{EW}^C$  are often assumed to be small, which is conceptually not appropriate as  $P_{EW}^C$  is directly involved in Eq.(5). Furthermore, it provides a cancellation to the low isospin  $I = 0(1=2)$  part of  $P_{EW}$ . Thus its effects could be significant.

The suppression of  $R$  may require significant contributions from subleading diagrams such as annihilation diagram  $A$  or color-suppressed electro-weak penguin diagram  $P_{EW}^C$ . Considering the fact that  $A$  contributes to  $K^0$  and  $^0K$  in the same way, namely they have the same  $A \rightarrow P$  interference, one expects that an enhancement of  $A$  with appropriate strong phase can suppress simultaneously  $R$  and  $R_2$  while their effects would cancel in some extent in their ratio. The current data give

$$R_3 = \frac{2\text{Br}(^0K)}{\text{Br}(K^0)} = 1.0 \pm 0.08; \quad (6)$$

which agrees well with this conjecture. However an enhancement of  $A$  will lead to significant consequences to  $K \rightarrow K$  modes, especially  $K \rightarrow K^0$ , as it is not suppressed by CKM matrix element like in the  $K$  modes. It is expected that a strong constraint on  $A$  will be found once this decay mode is experimentally observed.

There already exists a number of global  $\chi^2$  analyses on  $B \rightarrow D_s^* \pi^0$ ;  $K$  and  $K \rightarrow K$  systems based on flavor SU(3) symmetry [12, 34, 39, 40, 41, 42]. But to trace back the origins of the above mentioned  $B \rightarrow D_s^* \pi^0$  and  $K$  puzzles, separate  $\chi^2$  analysis are urgently needed. Furthermore, the SU(3) breaking scheme dependences are not carefully examined in the previous analyses, which may lead to different results in the literature. Finally, the contributions from subleading diagrams such as  $P_{EW}^C$ ,  $E$ ,  $A$  and penguin induced annihilation diagram  $P_A$  which could play important roles in understanding the current data are often neglected.

The purpose of the present paper is to make an up to the date investigation on charmless B decays, following a strategy that first applying  $\chi^2$  analysis on  $B \rightarrow D_s^* \pi^0$ ,  $K$  and  $K \rightarrow K$  modes separately, then connecting them through flavor SU(3) symmetry and discuss the SU(3) breaking scheme dependency. After obtaining reasonable values of the dominant amplitudes, we then discuss their implications to  $K \rightarrow K$  modes with subleading diagrams such as  $P_{EW}^C$ ;  $E$ ;  $A$ ;  $P_A$  etc.

Our main observations are

Independent fits on  $B \rightarrow D_s^* \pi^0$  and  $K$  modes without SU(3) symmetry both favor a large ratio between color-suppressed tree (C) and tree (T) diagram, which disfavors the explanation of large nonfactorizable W-exchange diagrams (E). The extracted QCD penguin diagrams from  $B \rightarrow D_s^* \pi^0$ ,  $K$  and  $K \rightarrow K$  show a clear signal of SU(3) breaking and the breaking pattern is in agreement with naive factorization.

Global fits for  $B \rightarrow K$ ;  $K$  and  $K\bar{K}$  modes show good determinations of weak phase  $\delta$  in agreement with the standard model and prefer a larger electro-weak penguin ( $P_{EW}$ ) relative to  $T + C$  with a large strong phase when  $P_{EW}^C$  is neglected. The results are found stable among various SU(3) breaking schemes. The current data favor a SU(3) breaking scheme in which all the amplitudes for  $K$  are greater by a factor of  $f_K = f$  motivated from factorization.

An enhancement of  $P_{EW}^C$  with destructive interference to  $P_{EW}$  provides an alternative explanation to the small  $R_n$  within the SM. The suppression of  $R$  can be partially explained by an enhanced annihilation diagram  $A$ . The  $P_A$  provides a source of SU(3) breaking in strong phases.

The subleading diagrams may lead to significant CP violations in  $K\bar{K}$  modes. For typical value of  $A$  and  $P$ , the direct CP violation in  $K\bar{K}^0$  can reach  $\sim 0.4$ .

This paper is organized as follows. In section II, the basic formulas for diagrammatic decomposition are presented. In III, we extract the parameters such as weak phase  $\delta$  and the decay amplitudes from  $B \rightarrow K$ ,  $K$  and  $K\bar{K}$  modes separately. In section IV, we combine them in three different scenarios of SU(3) symmetry. One is that all the amplitudes in  $K$  modes are rescaled by a factor of  $f_K = f$  motivated from the naive factorization. Another one is that only the tree diagrams are rescaled by this factor while the rest of the amplitudes remain the same in SU(3) limit. The last one is the strict SU(3) limit. In section V, we consider the contributions from various subleading diagrams and extract their typical values. In section VI, the implications to the  $K\bar{K}$  modes are discussed. The possibility of finding large direct CP violations is indicated. We conclude in section VII.

## II. DIAGRAMMATIC DESCRIPTION

We use the following definitions for branching ratios and direct CP violations

$$\begin{aligned} \text{Br} &= \frac{1}{2} (A^2 + \bar{A}^2); \\ a_{CP} &= \frac{\bar{A}^2 - A^2}{\bar{A}^2 + A^2}; \end{aligned} \quad (7)$$

where  $A$  ( $\bar{A}$ ) stands for  $B^0$  ( $\bar{B}$ ) or  $B^+$  ( $\bar{B}$ ) decay amplitude.  $\Omega$  is a phase space factor,  $\Omega = 1$  for neutral final states and  $\Omega = \Omega_{B^+} = \Omega_{B^0} = 1.086 \pm 0.017$  for charged final states. The mixing induced CP violation parameters  $S$  and  $C$  are introduced through the time-dependent decay rate difference

$$\begin{aligned} a_{CP}(t) &= \frac{(B^0 \rightarrow f_{CP}) - (B^0 \rightarrow \bar{f}_{CP})}{(B^0 \rightarrow f_{CP}) + (B^0 \rightarrow \bar{f}_{CP})} \\ &= S \sin(m_B t) - C \cos(m_B t); \end{aligned} \quad (8)$$

with  $f_{CP}$  denoting final states with definite CP parities.  $m_B$  is the neutral  $B$  meson mass difference. The two parameters can be written as

$$S = \frac{2\text{Im}}{1 + \bar{A}^2}; \quad C = \frac{1 - \bar{A}^2}{1 + \bar{A}^2} = -a_{CP}; \quad (9)$$

with

$$= e^{2i \frac{A}{A}}; \quad (10)$$

in the SM .

Using the phase definitions of  $B^+ = (ub)$ ,  $B^0 = (db)$ ,  $K^+ = (us)$ ,  $K^0 = (ds)$  and  $\bar{K}^+ = (ud)$ ;  $\bar{K}^0 = (dd - uu)/2$ ;  $\bar{K}^0 = (ud)$ , one arrives at the following diagrammatic decompositions for  $B$  modes

$$\begin{aligned} A(B^+) &= (T + E + P + P_A + \frac{2}{3}P_{EW}^C); \\ A(B^0) &= \frac{1}{2}(C - E - P - P_A + P_{EW} + \frac{1}{3}P_{EW}^C); \\ A(\bar{K}^0) &= \frac{1}{2}(T + C + P_{EW} + P_{EW}^C); \end{aligned} \quad (11)$$

Similarly, the  $K$  modes are given by

$$\begin{aligned} A(K^+) &= (T^0 + P^0 + \frac{2}{3}P_{EW}^{C^0}); \\ A(K^0) &= \frac{1}{2}(C^0 - P^0 + P_{EW}^0 + \frac{1}{3}P_{EW}^{C^0}); \\ A(\bar{K}^0) &= A^0 + P^0 - \frac{1}{3}P_{EW}^{C^0}; \\ A(K^0) &= \frac{1}{2}(T^0 + C^0 + A^0 + P^0 + P_{EW}^0 + \frac{2}{3}P_{EW}^{C^0}); \end{aligned} \quad (12)$$

The amplitudes for  $K$  modes are marked by a prime, which equal to the unprimed ones for  $B$  modes in favor SU(3) limit. The  $KK$  modes are given by

$$\begin{aligned} A(K^+K^+) &= (E^0 + P_A^0); \\ A(K^0K^0) &= P^0 - \frac{1}{3}P_{EW}^{C^0} + P_A^0; \\ A(K^+K^0) &= P^0 - \frac{1}{3}P_{EW}^{C^0} + A^0; \end{aligned} \quad (13)$$

where the subleading diagrams such as color-suppressed electro-weak penguin ( $P_{EW}^C$ ),  $W$  exchange diagram ( $E$ ), annihilation diagram  $A$  and penguin-induced annihilation diagram ( $P_A$ ) are included. In the above formulas, the penguin exchange diagram ( $P_E$ ) are absorbed into penguin diagrams and the electroweak and color suppressed electroweak penguin exchange diagrams are neglected.

We start with independent analyzes on  $B$ ,  $K$  and  $KK$  modes. In the first step, all subleading diagrams such as  $P_{EW}^C$ ,  $E$ ,  $P_A$  and  $A$  are switched off for the reason of simplicity. Their effects will be investigated in detail in section IV and V. To consistently include the experimental errors of the data, the  $\chi^2$  method is adopted for extracting the decay amplitudes. The definition of  $\chi^2$  reads

$$\chi^2 = \sum_i \frac{f_i^{theo} - f_i^{exp}}{f_i^{exp}}{}^2; \quad (14)$$

where  $f_i^{\text{theo}}$  are the theoretical values of observables  $f_i$  ( $i = 1; m$ ) and  $f_j$  ( $j = 1; n$ ) are the to-be-determined parameters.  $f_i^{\text{exp}}$  and  $\delta_i$  are the experimental central values and errors. The best-fit of the parameters correspond to the minimum of the  $\chi^2$  function which satisfies a  $\chi^2$  distribution with degree-of-freedom (d.o.f)  $m - n$ . For the experimental data we take the values listed in Tab.I which are the weighted average of CLEO, Babar and Belle collaboration results[28]. Other major parameters used in the fits involve the CKM matrix element of

$$V_{cb} = 0.04 \pm 0.02; \quad V_{ub} = (3.9 \pm 0.68) \times 10^{-3}; \quad (15)$$

and the SM value of

$$\sin 2\beta = 0.73 \pm 0.037; \quad (16)$$

All the BRs are written in units of  $10^{-6}$ , and the angles are in gradient and arranged in the range  $(-\pi; +\pi)$ .

### III. ANALYSIS WITHOUT FLAVOR SU(3) SYMMETRY

#### A. $B \rightarrow \pi$ modes

The hierarchies in the decay amplitudes are controlled by both the Wilson coefficients and the CKM matrix elements. As the sizes of the CKM matrix elements are better known, it is helpful to factorize them out so that all the hadronic amplitudes in  $B \rightarrow \pi$ ,  $K$  and  $K_S$  etc have the same hierarchical structure. Thus we shall use the following parameterizations for  $B \rightarrow \pi$  modes

$$\begin{aligned} A(B^+ \rightarrow \pi^+) &= \frac{1}{\sqrt{2}} V_{ub} V_{ud} (T + E + P + P_A - P_{EW}) + \frac{1}{\sqrt{2}} V_{cb} V_{cd} (P + P_A + \frac{2}{3} P_{EW}^C); \\ A(B^0 \rightarrow \pi^0) &= \frac{1}{\sqrt{2}} V_{ub} V_{ud} (C - E + P + P_A - P_{EW} - \frac{1}{3} P_{EW}^C) + \frac{1}{\sqrt{2}} V_{cb} V_{cd} (P - P_A + P_{EW} + \frac{1}{3} P_{EW}^C); \\ A(B^0 \rightarrow \pi^0) &= \frac{1}{\sqrt{2}} V_{ub} V_{ud} (T + C - P_{EW} - P_{EW}^C) + \frac{1}{\sqrt{2}} V_{cb} V_{cd} (P_{EW} + P_{EW}^C); \end{aligned} \quad (17)$$

with  $V_{ub} V_{ud} = A^3(\theta_{12})$  ( $\theta_{12}^2=2$ ), and  $V_{cb} V_{cd} = A^3$ . Throughout the present paper, we shall assume the  $t$ -quark dominance in penguin type diagrams. In general a penguin diagram can be written as

$$P = V_{ub} P_u + V_{cb} P_c + V_{tb} P_t = V_{ub} P_{tu} + V_{cb} P_{tc}; \quad (18)$$

where  $P_{tu} = P_t - P_u$  and  $P_{tc} = P_t - P_c$ . The  $t$ -quark dominance in the Wilson coefficient then leads to  $P_t = P_c = P_u$  and

$$P_{tu} = P_{tc} = P_t = P: \quad (19)$$

Note that in the presence of large charm ing penguin [43, 44, 45],  $P_{tc}$  could differ from  $P$ . This effect can be effectively absorbed into inelastic final state interactions (FSIs) and will not be discussed in detail here.

From the isospin structure of the low energy effective Hamiltonian, the sum  $T + C$  and  $P_{EW} + P_{EW}^C$  have both isospin  $I = 2$ . It is then helpful to define

$$\hat{T} = T + C; \quad \hat{P}_{EW} = P_{EW} + P_{EW}^C : \quad (20)$$

The ratio  $R_{EW}^{SM}$  is just the ratio of the isospin  $I = 2$  part between electroweak penguin and tree diagrams.

In the naive factorization approach [5, 6], these amplitudes have the following typical values

$$\begin{aligned} T &= 0.9 \quad 1.1; & C &= 0.33 \quad 0.25; \\ P &' 0.1; & P_{EW} &= 0.013 \quad 0.015; \\ P_{EW}^C &= 0.0023 \quad 0.003; & & \end{aligned} \quad (21)$$

All the amplitudes are almost real. The ranges of the parameters correspond to the effective number of color  $N_c$  ranging from 2 to infinity. In the factorization approach, the rescaled amplitudes satisfy a hierarchy of

$$|T_j| \gg |P_j| \gg |P_{EW}| \gg |P_{EW}^C| \quad (22)$$

which holds for all primed and double-primed amplitudes in  $K$  and  $K\bar{K}$  modes.

Including the time dependent CP asymmetry, the  $\chi^2$  minimization provides seven data points. A direct fit to the data gives the following best fits corresponding to a local minimum of  $\chi^2$  function.

$$\begin{aligned} |T_j| &= 0.53^{+0.036}_{-0.031}; & |C_j| &= 0.42^{+0.081}_{-0.11}; \\ c &= 0.84^{+0.57}_{-0.41}; & |P_j| &= 0.099^{+0.038}_{-0.045}; \\ p &= 0.55^{+0.27}_{-0.73}; & \phi &= 1.1^{+0.26}_{-0.29}; \end{aligned} \quad (23)$$

with  $\chi^2_{min} = dof = 0.17 = 1$ , where  $P_{EW}$  is fixed relative to  $\hat{T}$  through Eq.(5). The above result show that:

The  $\chi^2$  data prefer a large  $|C_j| = T_j = 0.8 \quad 0.2$ , which is in contradiction with the factorization based estimation. This is not new, however we note that the a large relative strong phase of  $c = 0.84$  is also obtained, which disagrees with a recent calculation based on soft collinear effective theory claiming that  $\text{Im}(C=T)$  should be vanishing at leading order [46]. The large  $|C_j|$  and its strong phase  $c$  are required by the observed two ratios in Eq.(3). In the following figure (Fig.1), the dependences of the ratios with  $|C_j| = T_j$  and  $c$  are given. For illustration purpose, we fix other parameters to be  $|T_j| = 0.53$ ,  $|P_j| = 0.1$ ,  $p = 0.55$  and  $\phi = 1.1$ , corresponding to their best fits.

It follows from Fig. 1 that both  $R_+$  and  $R_{00}$  prefer a large  $|C_j| = T_j$  around 0.8. There is very little dependence on  $c$  for  $R_{00}$ . However, the large strong phase of  $c' = 1.0$  is required by  $R_+$ , namely by the interference between  $T$  and  $C$  in  $\chi^0$  mode.

The determination of  $\phi$  is in agreement with the SM fit. However, in  $\chi^0$  system, there could be multiple solutions [17, 47]. The  $\chi^2$  curve as function of  $\phi$  is give in Fig3, which also indicates a local minimum of  $\chi^2$  close to  $\phi = 0.23$ . But the corresponding

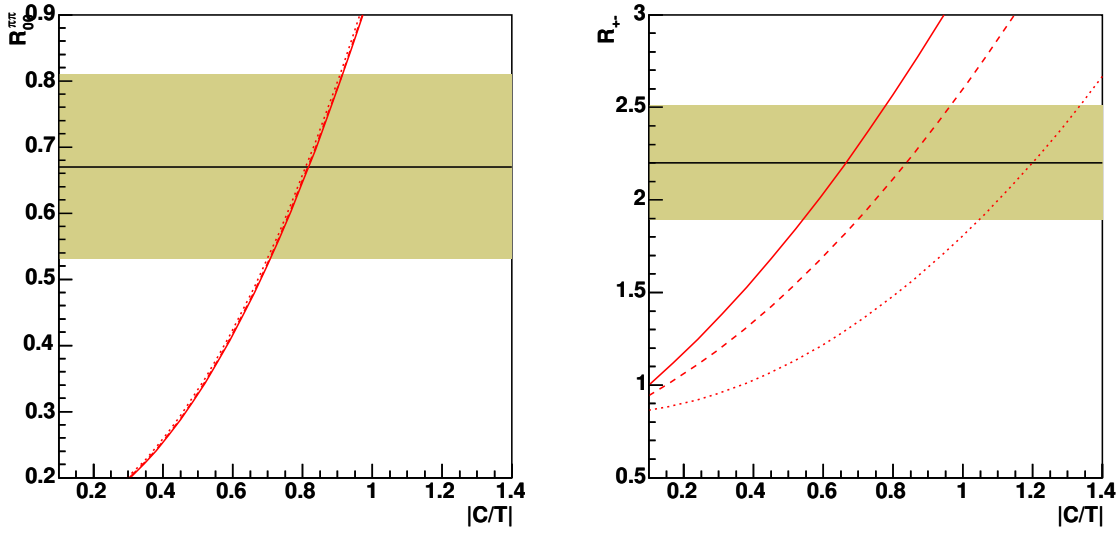


FIG .1:  $R_{00}$  and  $R_+$  as functions of  $|C/T|$  with different value of  $c$ . The three curves correspond to  $c = 0.5; 1.0; 1.5$  respectively. The shadowed bands are the experimentally allowed ranges. The other parameters are fixed at their best fitted value in Eq.(23)

best fitted other parameters are  $|T|j' = 0.3$ ,  $|C|j' = 0.84$ ,  $c' = 1.7$  and  $|P|j' = 0.36$  which looks unreasonable as it favors  $|C|j$   $|T|j$  and  $|T|j'$   $|P|j$ . To get rid of the multi-solutions, one may include the  $K$  modes via favor  $SU(3)$  symmetry. The simplest way is to include  $^+K$  mode only, as it was done in Ref.[2]. The two-fold ambiguity in  $\ln$  can be easily lifted.

The value of  $|P|j' = 0.1$  agrees well with naive factorization estimate in Eq(21) while  $T$  is suppressed. The enhancement of  $C$  and suppression of  $T$  implies that there could be a mixing between a diagram and its color-suppressed counterpart. For  $\pi$  modes, it may be due to large FSI through  $B \rightarrow \pi^+ (\pi^0 \pi^0) \rightarrow \pi^0 \pi^0 (\pi^+ \pi^-)$ . A recent calculation based on one particle exchange model indeed supports this conjecture [14]. Such a mixing may also apply to  $D^0 \pi^0$  and  $\pi^0 \pi^0$  modes.

## B. $K$ modes

The amplitudes of  $K$  modes are written in a similar way

$$\begin{aligned}
A(+K) &= \frac{1}{\sqrt{2}} \left( \frac{s_u}{\sqrt{2}} (\Gamma^0 + P^0 + \frac{2}{3} P_{EW}^{C^0}) + \frac{s_c}{\sqrt{2}} (P^0 + \frac{2}{3} P_{EW}^{C^0}) \right); \\
A(0\bar{K}^0) &= \frac{1}{\sqrt{2}} \left( \frac{s_u}{\sqrt{2}} (C^0 + P^0 + P_{EW}^0 + \frac{1}{3} P_{EW}^{C^0}) + \frac{s_c}{\sqrt{2}} (P^0 + P_{EW}^0 + \frac{1}{3} P_{EW}^{C^0}) \right); \\
A(\bar{K}^0) &= \frac{s_u}{\sqrt{2}} (A^0 + P^0 + \frac{1}{3} P_{EW}^{C^0}) + \frac{s_c}{\sqrt{2}} (P^0 + \frac{1}{3} P_{EW}^{C^0}); \\
A(0K) &= \frac{1}{\sqrt{2}} \left( \frac{s_u}{\sqrt{2}} (\Gamma^0 + C^0 + A^0 + P^0 + P_{EW}^0 + \frac{2}{3} P_{EW}^{C^0}) + \frac{s_c}{\sqrt{2}} (P^0 + P_{EW}^0 + \frac{2}{3} P_{EW}^{C^0}) \right);
\end{aligned} \tag{24}$$

with  $\frac{s_u}{\sqrt{2}} = V_{ub}V_{us} = A^4(\lambda^4)$ , and  $\frac{s_c}{\sqrt{2}} = V_{cb}V_{cs} = A^2(1 - \lambda^2)$ . Note that in the  $K$  modes  $j_u^s$  is much smaller than  $j_c^s$ ,  $j_u^s = \frac{s_u}{\sqrt{2}} j_c^s \approx 0.02$ . The suppression of the tree-penguin interference and the limited accuracy of the present data make it less effective to extract the weak phase from  $K$  modes at the present stage. Thus if one considers  $K$  modes alone, it is more useful to take as known from the global SM fit to explore the other hadronic decay amplitudes. Taking the SM value of  $\lambda = 1.08^{+0.17}_{-0.21}$  as input and also fixing the  $P_{EW}^0$  with the SM relation of Eq.(5), one finds the following solution

$$\begin{aligned}
\mathcal{T}^0 j &= 1.54^{+0.61}_{-0.38}; \quad \mathcal{C}^0 j = 2.7^{+0.61}_{-0.7}; \\
c^0 &= 3.1 \pm 0.11; \quad \mathcal{P}^0 j = 0.12 \pm 0.0023; \\
P^0 &= 0.2^{+0.07}_{-0.12};
\end{aligned} \tag{25}$$

with a  $\chi^2/\text{d.o.f} = 2.49/4$ . From the above result, one arrives at the following observations

The  $K$  data favor both large  $\mathcal{T}$  and  $C^0$  with an even larger ratio of  $\mathcal{C}^0 = \mathcal{T}^0 j = 1.75 \pm 0.7$ . Although the errors are considerably large, it is evident that a large  $\mathcal{C}^0 = \mathcal{T}^0 j \approx 0(1)$  is also favored in  $K$  modes. A similar observation was made in Ref.[48] where no error estimation was given. The large  $\mathcal{C}^0 = \mathcal{T}^0 j$  is due to the suppression of  $R_n$  from unity, in Fig 2 the value of  $R_n$  as function of  $\mathcal{C}^0 = \mathcal{T}^0 j$  is plotted, one sees that in general, a large  $\mathcal{C}^0 = \mathcal{T}^0 j$  with large relative strong phase  $c^0 \approx 2$  can lead to the reduction of the ratio  $R_n$ .

$\mathcal{P}^0$  is well determined which is about 20% larger than  $P$ , in a good agreement with the factorization based estimation that  $P^0 = P' f_K = f' 1.28$ .

A relatively larger  $\chi^2/\text{d.o.f}$  in  $K$  fit indicates larger inconsistency with the data in comparison with that for  $\pi$  modes. The sources of inconsistency mainly come from  $Br(+K)$  and  $Br(0\bar{K}^0)$  and also  $S(0K_S)$ . The best fit prefers a larger value of  $R_n \approx 0.9$  and a very small  $S(0K_S) \approx 0.02$ .

An alternative way to achieve at a smaller  $R_n$  is to allow  $P_{EW}$  to be larger, which needs new physics effects beyond the SM. Taking  $P_{EW}$  to be free, one finds

$$\begin{aligned}
\mathcal{T}^0 j &= 2.75^{+1.12}_{-1.38}; \quad \mathcal{C}^0 j = 1.31^{+0.71}_{-0.75}; \\
c^0 &= 2.76 \pm 0.28; \quad \mathcal{P}^0 j = 0.12 \pm 0.0023; \\
P^0 &= 0.08^{+0.02}_{-0.08}; \quad \mathcal{P}_{EW}^0 j = 0.048 \pm 0.02; \\
P_{EW}^0 &= 1.44^{+0.08}_{-0.13};
\end{aligned} \tag{26}$$

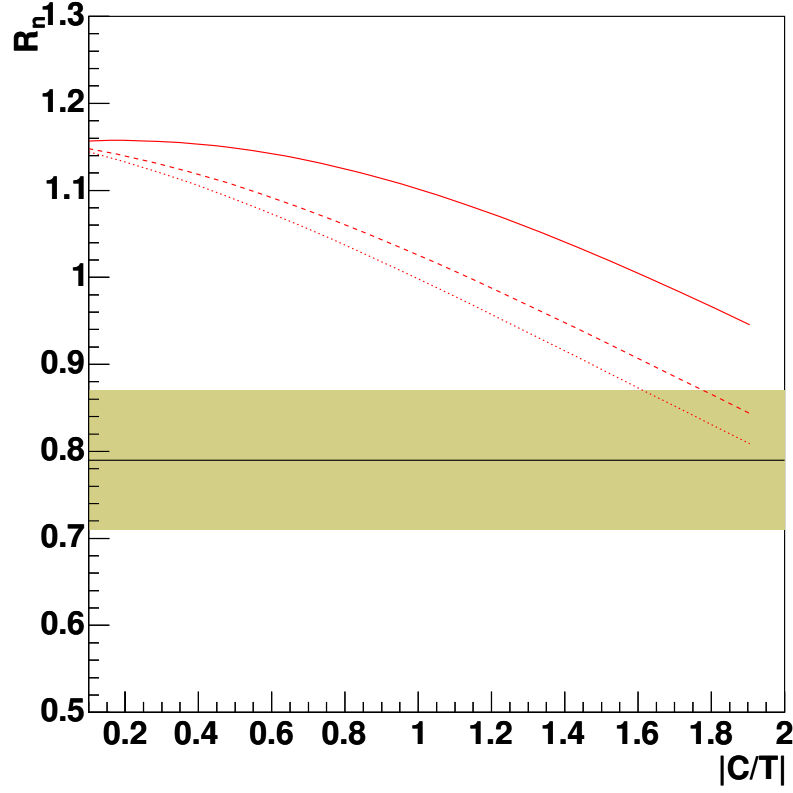


FIG. 2:  $R_n$  as functions of  $|C/T|$  with different value of  $c_0$ . The three curves correspond to  $c_0 = 1.0; 2.0; 3.0$  respectively. The shadowed band is the experimentally allowed range.

with  $\Delta = \text{diff} = 0.4 = 2$ . Indeed, one sees that a large  $P_{EW}^0$  is favored by the  $K$  data with  $P_{EW}^0 = (T^0 + C^0)j = 0.04 \sim 0.04$ . Once  $P_{EW}^0$  is increasing, the ratio of  $C^0 = T^0$  decreases. It seems to be a promising way to restore a reasonable value of  $C^0 = T^0$ . However, it only holds for  $K$  modes. Furthermore, the uncertainties are too large to prevent us to draw any robust conclusion on that. The precisions can be improved significantly by making use of the whole charmless  $B$  decay data connected by flavor  $SU(3)$  symmetry.

It is more difficult to explain the suppression of  $R$  in  $^+K$  and  $K^0$  modes, as both  $C$  and  $P_{EW}$  are absent. If the puzzle of  $R$  has to be taken seriously, one needs an enhancement of either  $A$  or  $P_{EW}^C$ . This possibility will be discussed in sections IV and V.

### C. $KK$ modes

For the  $KK$  modes, currently only  $K^0K^0$  mode has been observed. The decay amplitude is given by

$$A(K^0K^0) = \frac{1}{\sqrt{2}} \left( P^{\omega} + \frac{1}{3} P_{EW}^{C\omega} - P_A^{\omega} \right) - \frac{1}{\sqrt{2}} \left( P^{\omega} - \frac{1}{3} P_{EW}^{C\omega} + P_A^{\omega} \right); \quad (27)$$

which is dominated by QCD penguin (through  $b \rightarrow d$ ). Neglecting all subleading diagrams  $P_{EW}^C$  and  $P_A$ , one can directly extract the amplitude of penguin from the data

$$P^0_j = 0.2^{+0.4}_{-0.3}; \quad (28)$$

where we have taken the SM value of  $\alpha_s$  as input. It is evident that the QCD penguins for  $\pi$ ,  $K$  and  $KK$  follow a pattern

$$P_j \cdot P^0_j \cdot P^0_j; \quad (29)$$

and roughly agrees with a factorization based estimation in that the SU(3) breaking effects are proportional to the decay constants of the final states, namely

$$\frac{P^0}{P} = \frac{P^0}{P^0} = \frac{f_K}{f}; \quad (30)$$

Thus one finds that a separate analysis can indeed provide important information on decay amplitudes and test SU(3) symmetry breaking, which can not be obtained by a global  $\chi^2$  analysis.

#### IV. ANALYSIS USING FLAVOR SU(3) SYMMETRY

##### A. Fit within SM

We are in the position now to connect the  $\pi$ ,  $K$  and  $KK$  modes through approximate flavor SU(3) symmetry. Note that there is no reliable way to estimate the size of the SU(3) breaking in theory. From the factorization based approaches the SU(3) breaks in such a way that the amplitudes in  $KK$  modes differ from the ones in  $(K)$  modes by a factor of  $f_K = f$ , where  $f_K$  and  $f$  are decay constants for  $K$  and  $\pi$  mesons. There have been analysis based on different patterns of SU(3) breaking which could in general lead to different results. Here we would like to consider three scenarios of SU(3) relations frequently used in the literature:

Scenario A) All diagrammatic amplitudes for  $KK$  modes are larger than that in  $(K)$  modes by a factor  $f_K = f$ .

$$\frac{T^0}{T} = \frac{C^0}{C} = \frac{P^0}{P} \quad \frac{T^0}{T^0} = \frac{C^0}{C^0} = \frac{P^0}{P^0} = \frac{f_K}{f}; \quad (31)$$

Scenario B) SU(3) symmetry breaks only in tree diagrams [40, 41]

$$\frac{T^0}{T} = \frac{T^0}{T^0} = \frac{f_K}{f}; \quad \frac{C^0}{C} = \frac{P^0}{P} \quad \frac{C^0}{C^0} = \frac{P^0}{P^0} = 1; \quad (32)$$

Scenario C) Exact SU(3) limit

$$\frac{T^0}{T} = \frac{C^0}{C} = \frac{P^0}{P} \quad \frac{T^0}{T^0} = \frac{C^0}{C^0} = \frac{P^0}{P^0} = 1; \quad (33)$$

As in the first step, the  $P_{EW}$  is fixed within the SM through Eq.(5). Thus there are 6 parameters  $T, C, C, P, P$  and  $\alpha_s$  to be fitted by 18 data points. The best-fitted parameters as well as the  $B$  rs and  $a_{CP}$  s are tabulated in Tab.II.

The results show that:

	scenario A	scenario B	scenario C
$\mathcal{T} j$	0:52 0:027	0:51 0:033	0:52 0:032
$\mathcal{J} j$	0:47 0:042	0:45 0:053	0:45 0:053
$c$	1:1 0:19	$1^{+0:21}_{0:19}$	$1:1^{+0:21}_{0:19}$
$\mathcal{P} j$	0:094 0:0014	0:12 0:0019	0:12 0:0018
$P$	$0:49^{+0:089}_{0:1}$	$0:45^{+0:087}_{0:11}$	$0:54^{+0:11}_{0:13}$
$\mathcal{P}_{EW} j$	0:011 0:0011	0:011 0:0011	0:011 0:0011
$P_{EW}$	0:52 0:1	0:47 0:11	0:49 0:11
$\chi^2_{min} = dof$	$1^{+0:11}_{0:13}$ 16.2/12	$1:1^{+0:13}_{0:17}$ 19.2/12	$1:1^{+0:14}_{0:17}$ 21/12
$Br(+)$	4:7 0:48	4:8 0:62	4:9 0:59
$a_{CP}(+)$	0:27 0:062	0:32 0:085	0:37 0:096
$Br(0^0)$	1:7 0:31	1:8 0:4	1:8 0:41
$a_{CP}(0^0)$	0:36 0:11	0:43 0:15	0:38 0:17
$Br(0)$	5:2 0:77	5:1 0:85	5:1 0:86
$a_{CP}(0)$	0 0:01	0 0:01	0 0:01
$Br(+K)$	20 0:77	20 0:84	20 0:74
$a_{CP}(+K)$	0:1 0:02	0:097 0:022	0:089 0:019
$Br(0K^0)$	9:8 0:49	9:9 0:47	9:7 0:46
$a_{CP}(0K^0)$	0:1 0:035	0:076 0:03	0:068 0:032
$Br(K^0)$	22 0:69	22 0:71	22 0:68
$Br(0K)$	12 0:63	11 0:64	12 0:57
$a_{CP}(0K)$	0:0055 0:042	0:016 0:039	0:014 0:04
$Br(K^0K^0)$	1:3 0:17	2:3 0:35	0:84 0:13
$Br(KK^0)$	1:3 0:17	2:3 0:35	0:84 0:13
$S(+)$	0:73 0:13	0:76 0:13	0:73 0:14
$S(0^0)$	0:23 0:27	0:51 0:27	0:52 0:27
$S(K^0K^0)$	0:86 0:038	0:84 0:04	0:84 0:04

TABLE II: Global fit to  $\tau \rightarrow K$  and  $KK$  modes within SM. The three columns corresponds to the three different SU(3) relations used in the fits.

The differences among the three scenarios are in general not large. The weak phase  $\beta$  is well determined in all the cases and depends on the SU(3) breaking scheme very weakly. All the three scenarios give  $\beta \approx 1:1$  in a good agreement with the SM value with differences less than 10%, which manifests that  $\beta$  can be reliably extracted using the diagrammatic approach. The  $\chi^2_{min}$  curves as function of  $\beta$  are given in Fig.3. Comparing with the one from [1], one finds a significant improvement on the precision of  $\beta$  determination. The three patterns lead to roughly the same  $\mathcal{T} j$  and  $\mathcal{J} j$  with  $\mathcal{J} = \mathcal{T} j' \approx 0:8$ . Note that for small  $\mathcal{J} j$  we find no consistent fit. For example, if  $\mathcal{J} j$  is fixed at  $C = 0:2$ , a very big  $\chi^2_{min} = dof = 44:6=12$  is obtained. The major difference is the value of  $\mathcal{P} j$ . The scenario B) and C) prefer a  $\mathcal{P} j$  which is 20% larger.

Among the three cases, the scenario A) that all the primed (double-primed) amplitudes are larger than the unprimed (primed) ones by a factor of  $f_K = f$  gains the lowest  $\chi^2 = 16.2 = 12$ , which indicates a better consistency in comparison with the other two. The exact SU(3) scenario gains the largest  $\chi^2 = 21 = 12$ , which clearly indicates that the flavor SU(3) symmetry in charmless B decays must be a broken one.

The main source of the inconsistency comes from the  $Br(K^+ K^-)$ ,  $Br(K^0 \bar{K}^0)$  and  $Br(K^+ \bar{K}^0)$ . The best fits in scenario A prefer a larger  $Br(K^+ K^-) \sim 20$ , a small  $Br(K^0 \bar{K}^0) \sim 9.8$  and a small  $Br(K^+ \bar{K}^0) \sim 22$ . Namely, within the current parameterization, it is not possible to arrive at the observed ratios  $R_n$  and  $R_2$ . Thus the  $K$  puzzles remain.

For the predictions for the  $KK$  modes, the scenario A gives  $Br(K^0 K^0) = Br(K^+ K^-) = 1.2$ , while the other two give 1.7 (scenario B) and 0.84 (scenario C) respectively. The branching ratio of  $K^+ K^-$  is predicted to be zero and all the predicted direct CP violation are vanishing, due to the lack of interferences between amplitudes.

Other possibilities of SU(3) breaking include the SU(3) breaking in strong phases, which has been discussed in Refs.[33]. The current data favor a small SU(3) breaking in the strong phase of QCD penguin. This breaking effect can significantly modify the correlation of direct CP asymmetries between  $K^+ K^-$  and  $K$  modes [2].

#### B. Fit with free electroweak penguin $P_{EW}$

In the next step, we consider the possibility that  $P_{EW}$  is free from the SM constraint. The fitting results with free  $P_{EW}$  under three scenarios are given in Tab.III.

In this case, one finds that all the fits prefer a larger value of  $\hat{P}_{EW} = 0.23 \sim 0.29$  with a large strong phase  $\phi_{P_{EW}} = 0.6 \sim 0.7$  relative to  $\hat{T}$  as the corresponding best fit of  $\hat{T}$  has a strong phase of  $0.5 \sim 0.4$ . A large  $\hat{P}_{EW}$  with a large strong phase relative to  $\hat{T}$  can naturally explain the suppression of  $R_n$  and also  $R_2$  [2, 18, 19, 20, 35, 36, 37, 38]. Naively speaking, all  $K$  modes are QCD penguin dominant, the ratios  $R_n$  and  $R_2$  should be very close to unity. The corrections arise from either tree type diagrams or electroweak penguins. The former is CKM suppressed in  $K$  modes and is constrained by  $R_n$  data. Thus an enhancement of electroweak penguin is needed.

As the two ratios  $R_n$  and  $R_2$  are both  $P_{EW}$  sensitive, they can be used as probes of electro-weak penguins. We parameterize the deviation of SM by introducing a complex parameter

$$\frac{\hat{P}_{EW}}{\hat{T}} = R_{EW}^{SM} \quad : \quad (34)$$

In Fig.5, the two ratios are plotted with different values of  $j$  and its strong phase  $\phi_j$ . For demonstration reasons, the other parameters are fixed at the best fitted values in SM in the first column of Tab. II according to the scenario A, namely

$$T = 0.52; \quad C = 0.47; \quad c = 1.1; \quad P = 0.094 \quad \text{and} \quad \phi_P = 0.49: \quad (35)$$

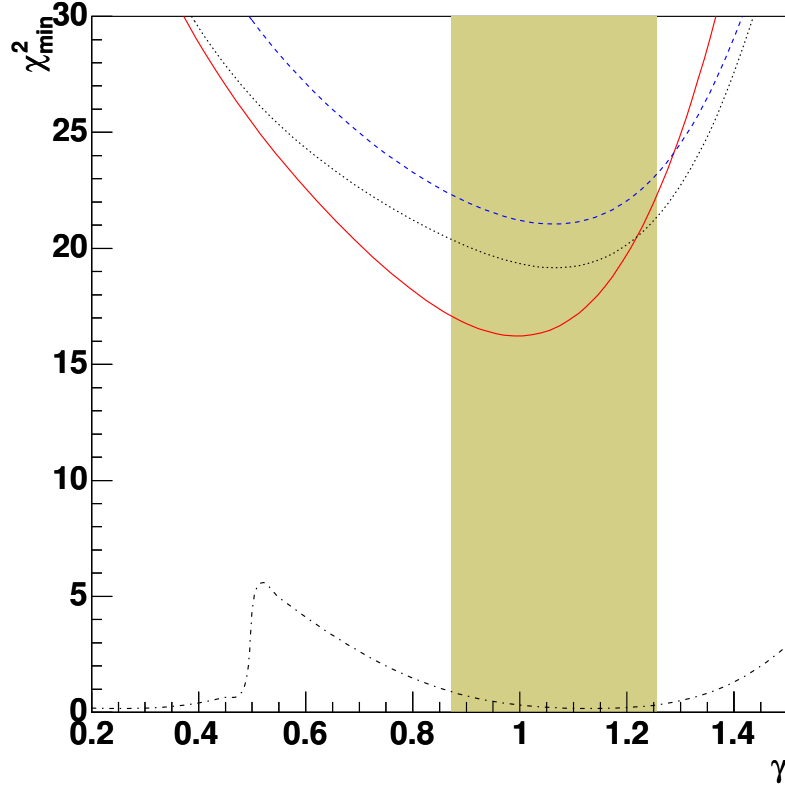


FIG. 3:  $\chi^2_{\min}$  as functions of weak phase  $\gamma$ . The three upper curves correspond to the three fits in Tab. II. The solid, dashed and dotted curves correspond to scenario A, B and C respectively. The lower curve (dot-dashed) corresponds to the fit only to  $m$  modes in Eq.(23). The shadowed band is the allowed range from global SM fits.

The figures indicate strong dependences on  $\gamma$  and  $j \neq j'$  for both ratios. In the SM case, i.e.  $j \neq j' = 1$  and  $\gamma = 0$ ,  $R_n$  is expected to be above 1.0 in contrast with the experiment. For  $j \neq j' = 1$  and large  $\gamma = 1.5$ ,  $R_n$  is reduced but  $R_2$  is enhanced and departs away from the allowed range of the data. Thus to simultaneously explain both measurements, one needs a large  $j \neq j' = 2:0 \text{ -- } 3:0$  and a large strong phase of  $\gamma = 1:0 \text{ -- } 1:5$ . This observation is confirmed by the global fits with  $P_{EW}$  free in Tab. III which gives

$$\frac{P_{EW}}{\hat{T}} = \begin{matrix} < & (3:1 & 1:3)e^{i(1:02 \pm 0:5)} & 10^{-2} & \text{(scenario A)} \\ : & (4:8 & 1:5)e^{i(1:06 \pm 0:53)} & 10^{-2} & \text{(scenario B)} \\ & (3:1 & 1:5)e^{i(1:03 \pm 0:5)} & 10^{-2} & \text{(scenario C)} \end{matrix} \quad (36)$$

With  $P_{EW}$  being free, the best fitted  ${}^0K^0$  mode is found to be  $Br({}^0K^0) = 11 \pm 1:9$  in scenario A, in a remarkable agreement with the data. The central values of the two ratios are found to be  $R_n \approx R_2 \approx 0:9$ .

The enhanced  $P_{EW}$  with large strong phase will result in different predictions for the CP asymmetries. In most decay modes the predicted  $a_{CP}$ s are much smaller [2]. However, the most important one is  $a_{CP}({}^0K^0)$  which should be exactly zero in SM. But now it prefers

	scenario A	scenario B	scenario C
$\mathcal{T} j$	0:52 0:028	0:51 <sup>+0:037</sup> <sub>0:045</sub>	0:51 0:035
$\mathcal{C} j$	0:45 0:052	0:44 <sup>+0:096</sup> <sub>0:062</sub>	0:44 <sup>+0:078</sup> <sub>0:064</sub>
$c$	0:96 <sup>+0:23</sup> <sub>0:21</sub>	0:92 0:25	0:98 0:24
$\mathcal{P} j$	0:093 0:0015	0:12 0:0019	0:12 0:0019
$P$	0:52 <sup>+0:1</sup> <sub>0:13</sub>	0:49 <sup>+0:1</sup> <sub>0:24</sub>	0:59 <sup>+0:13</sup> <sub>0:22</sub>
$\mathcal{P}_{EW} j$	0:023 <sup>+0:0096</sup> <sub>0:011</sub>	0:027 0:014	0:029 0:013
$P_{EW}$	0:63 <sup>+0:21</sup> <sub>0:41</sub>	0:7 <sup>+0:23</sup> <sub>0:35</sub>	0:63 <sup>+0:23</sup> <sub>0:32</sub>
$1^{+0:13}$ <sub>0:18</sub>		1:1 <sup>+0:16</sup> <sub>0:36</sub>	1 <sup>+0:17</sup> <sub>0:26</sub>
$\frac{2}{m_{in}} = dof$	13.2/10	15.9/10	18/10
$Br(+)$	4:7 0:53	4:8 0:84	4:9 0:7
$a_{CP}(+)$	0:29 0:077	0:34 0:14	0:39 0:14
$Br(0^0)$	1:6 0:38	1:7 0:66	1:7 0:58
$a_{CP}(0^0)$	0:14 0:18	0:16 0:26	0:12 0:26
$Br(0)$	5:4 0:89	5:3 1:2	5:2 1:1
$a_{CP}(0)$	0:085 0:045	0:11 0:061	0:11 0:06
$Br(+K)$	20 0:85	20 1:1	20 0:84
$a_{CP}(+K)$	0:11 0:024	0:1 0:035	0:093 0:027
$Br(0K^0)$	11 1:9	11 1:8	11 1:9
$a_{CP}(0K^0)$	0:034 0:045	0:027 0:043	0:02 0:042
$Br(K^0)$	22 0:73	22 0:74	22 0:73
$Br(0K)$	12 2:2	12 2:2	12 2:2
$a_{CP}(0K)$	0:033 0:059	0:012 0:063	0:01 0:057
$Br(K^0K^0)$	1:3 0:21	2:3 0:56	0:81 0:17
$Br(KK^0)$	1:3 0:21	2:3 0:56	0:81 0:17
$S(+)$	0:7 0:17	0:73 0:22	0:71 0:2
$S(0^0)$	0:4 0:31	0:54 0:41	0:55 0:36
$S(K^0K^0)$	0:86 0:039	0:84 0:043	0:84 0:042

TABLE III: The same as Tab.II, but  $P_{EW}$  is taken as a free parameter to be determined directly from the data.

a negative value of  $a_{CP}(0)$   $< 0:1$ , which is in agreement with the current preliminary data of  $a_{CP} = 0:02 - 0:07$  and can be examined with more precise data in the near future.

It needs to be emphasized that the large  $P_{EW}$  here means a relative enhancement to tree type diagram  $\hat{T}$ , not to QCD penguin diagram. It was claimed recently in Ref. [13] that there was no clear indication of large  $P_{EW} = P$ , which does not necessarily contradict with the conclusions in the present paper. Furthermore, using the numerical value of  $T$  and  $C$  obtained in Ref. [13], we find a similar result as in Eq.(36). Note that the ratio  $P_{EW} = P$  is subjected to large theoretical uncertainties, it is better to use the values relative to  $\hat{T}$  for exploring the electro-weak penguin and new physics as it is free from hadronic uncertainties.

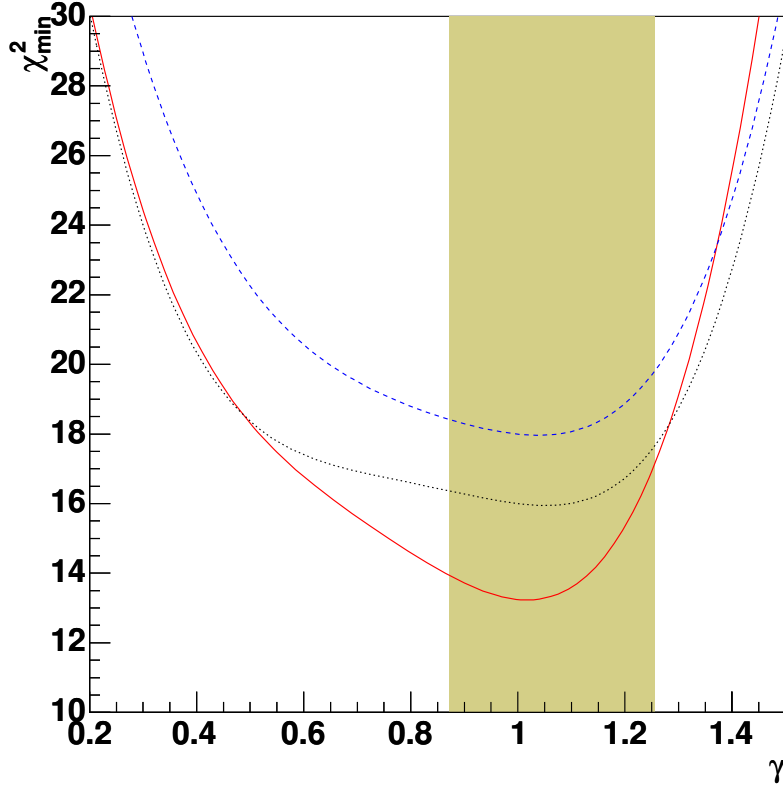


FIG .4:  $\chi^2_{\min}$  as functions of weak phase  $\gamma$ . The three upper curves correspond to the three  $t$  in Tab.III. The solid, dashed and dotted curves correspond to scenario A, B and C respectively. The shadowed band is the allowed range from global SM  $t$ .

### C . Effects of color suppressed electroweak penguin $P_{EW}^C$

In the previous discussions, the color-suppressed electroweak penguin diagram  $P_{EW}^C$  is neglected. However, among all the subleading diagrams  $P_{EW}^C$  is the only one giving contribution to high isospin state  $I = 2(3=2)$  in  $(K)$  modes. Furthermore, it cancels the isospin  $I = 0(1=2)$  components of  $P_{EW}$  just like C cancels that of T and directly contribute to the ratio in Eq.(5). Since the current data indicate a sizable C, it is still possible that there will be an enhancement of  $P_{EW}^C$  as well. In the SM,  $\hat{P}_{EW}^C$  is fixed relative to  $\hat{T}$ . However, given a large relative strong phase i.e negative interference between  $P_{EW}$  and  $P_{EW}^C$ , a large value of  $P_{EW}^C$  is possible within the SM. Note that the  $^0K^0$  mode depends on  $P_{EW} + P_{EW}^C = 3 = \hat{P}_{EW}^C = 3 + 2P_{EW} = 3$ . Even the first term is constrained by Eq.(5), the second term can still enhance the decay rate of  $^0K^0$  mode without violating the SM relation. The similar arguments also applies to  $^0K$  modes which depends on  $P_{EW} + 2P_{EW}^C = 3$ .

To see the effects of  $P_{EW}^C$ , we give in Fig.6, the ratios of  $R_1$  and  $R_2$  as function of  $P_{EW}^C$  and its strong phase  $\phi_{P_{EW}^C}$ . In the numerical calculations we take the values of other amplitudes from the SM  $t$ , according to the first column of Tab.II or Eq.(35). The values of  $P_{EW}$  and its strong phase are automatically generated from Eq.(5). It follows from the figure that for

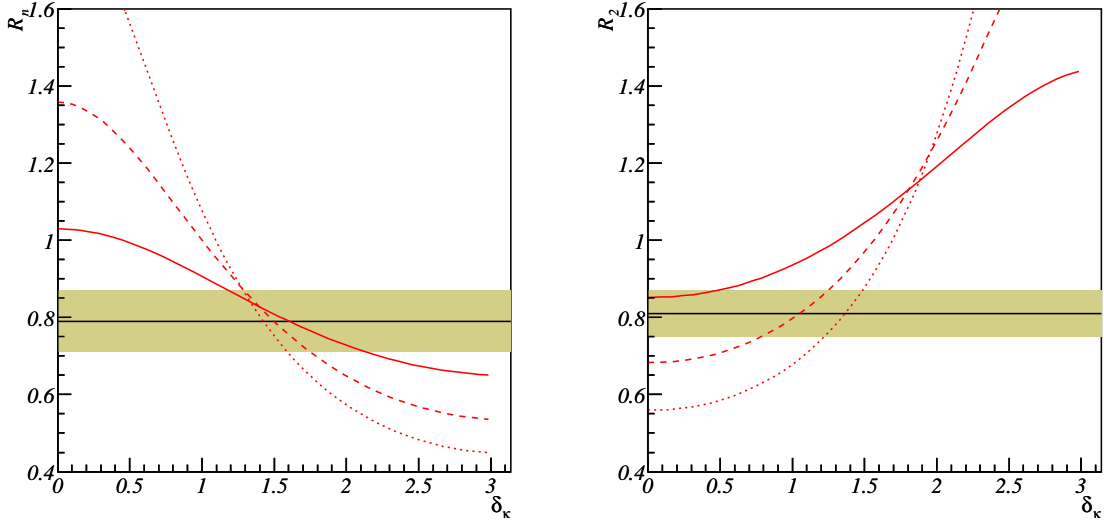


FIG. 5:  $R_n$  and  $R_2$  as function of  $\delta_k$  with different value of  $j$ . The three curves correspond to  $j = 1:0$  (solid);  $2:0$  (dashed);  $3:0$  (dotted). The shadowed bands are the experimentally allowed ranges. Other parameter are fixed at the SM best fitted values (column A in Tab.II).

a small  $P_{EW}^C \ll 0.1$  the predicted value of  $R_n$  is far above the data for all values of  $P_{EW}^C$ . To account for the current data  $P_{EW}^C$  has to be greater than  $0.4$ . The strong phase  $P_{EW}^C$  receives strong constraint from  $R_2$ . For  $P_{EW}^C$  in the range  $0.1 \sim 0.6$ , a large negative value of  $\phi_{EW}^C = 0.2 \sim 2.5$  is favored.

Including  $P_{EW}^C$  as a new free parameter while keep Eq.(5), we find

$$P_{EW}^C = 0.025 \quad 0.021; \quad P_{EW}^C = 2.24^{+0.21}_{-0.63} \quad (37)$$

and

$$\phi_{EW}^C = 0.03^{+0.02}_{-0.013}; \quad \phi_{EW}^C = 0.52^{+0.31}_{-0.72}; \quad (38)$$

with a  $\chi^2_{dof} = 11:3=10$ . The best fits of other parameters are listed in the first column of Tab.IV. Clearly, there is a strong cancellation in the sum of  $P_{EW} + P_{EW}^C$  as required by Eq.(5). It is of interest to note that for both tree and penguin diagrams the color suppressed diagrams are not necessarily suppressed. Furthermore, the current data suggest that

$$\frac{C}{T} \sim \frac{P_{EW}^C}{P_{EW}} \sim 0.8 \quad (39)$$

Thus the relative enhancements are likely to be universal. This is again in favor of the conjecture that it has a strong interaction origin which is flavor independent. Comparing with Eq.(40), one sees that  $P_{EW}^C$  is on the lower side to account for the suppression of  $R_n$ . The best fitted ratios are  $R_n \sim 0.89$  and  $R_2 \sim 0.78$  respectively. Thus a large  $P_{EW}^C$  improves the agreement with the data.

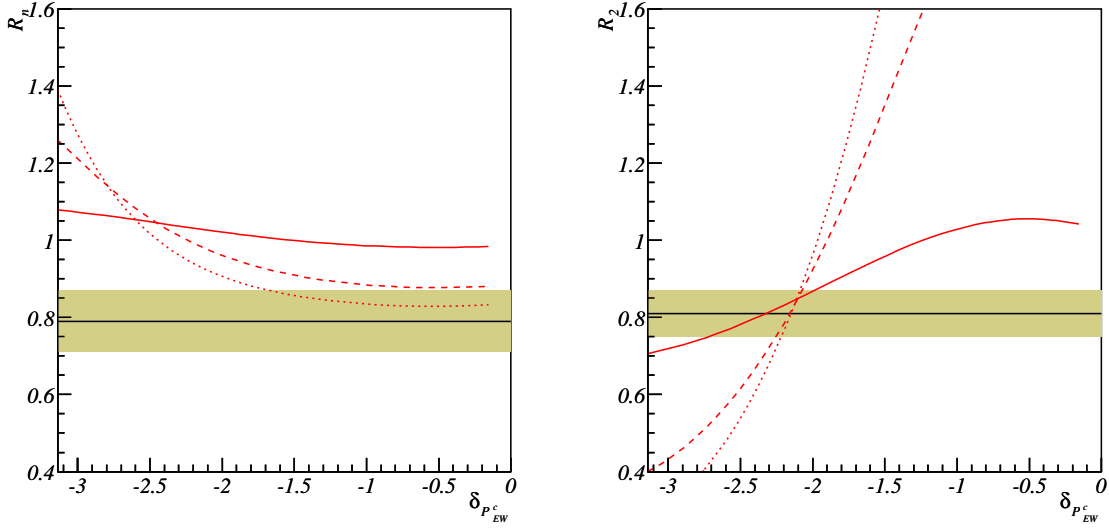


FIG. 6: Ratios of  $R_1$  and  $R_2$  as functions of  $\delta_{P_{EW}^C}$  and  $P_{EW}^C$ . The three curves correspond to  $P_{EW}^C = 0.01$  (solid),  $0.04$  (dashed) and  $0.06$  (dotted) respectively. Other parameters are fixed at their best fitted value in SM (according to column A of Tab.II). The shadowed bands are the allowed range by the current data.

Taking both  $P_{EW}$  and  $P_{EW}^C$  as independent free parameters, we get the following result

$$P_{EW}^C = 0.016 \pm 0.02; \quad P_{EW} = 2.59^{+0.4}_{-1.7} \quad (40)$$

and

$$P_{EW} = 0.027^{+0.016}_{-0.014}; \quad P_{EW}^C = 0.69^{+0.3}_{-0.6}; \quad (41)$$

with  $\chi^2_{min} = dof = 6:6=8$ . The color suppressed electroweak penguin is found to be reduced but still significant. In this case, all the  $K$  ratios are well reproduced. Note that the best fits correspond to  $P_{EW}^C = 0.032 \pm 0.018$  which again implies a violation of the SM relation.

Finally, we emphasize that the large  $P_{EW}^C$  within the SM may distinguish itself from the one beyond the SM by the prediction of direct CP violation in  $B \rightarrow \pi^0$  which should be vanishing in the former case and small but nonzero in the later.

Given a small  $P_{EW}^C$  relative to  $P_{EW}$ , the current data may imply new physics beyond the SM. New physics models significantly contributing to charmless  $B$  decays may include various SUSY models [22],  $Z^0$  models from extra  $U(1)$  gauge symmetry [21, 49] and two-Higgs-doublet models (2HDMs) [50]. Among various versions of two-Higgs-doublet models, the general 2HDM with spontaneous CP violation can provide rich sources of CP violation [51, 52, 53, 54, 55] and significant corrections to the electro-weak penguin through charge or neutral Higgs boson exchanges. The models with 4th generation may also give sizable contributions. Formodel with both two-Higgs-doublet and 4th generation quark, the effects could be more significant through neutral Higgs loops [56, 57, 58].

## V. NONFACTORIZABLE DIAGRAMS

We now go a step further to discuss the effects of other subleading nonfactorizable diagrams such as  $E$ ,  $A$  and  $P_A$ . They are expected to be very small from factorization based estimations. However, in the presence of large FSI, there could be mixing among diagrams which may enhance the sizes of subleading diagrams [25, 26, 27]. In view of the current puzzling pattern of the data, the possibility of anomalously large nonfactorizable diagrams can not be excluded.

Due to the limited number of data points, it is not possible to directly extract all of them simultaneously from the current data of  $\mathcal{B}(B \rightarrow K)$  and  $\mathcal{B}(B \rightarrow \bar{K})$ . Instead, to obtain the typical sizes of those diagrams, we shall consider several typical cases, in each case only one of the diagrams is assumed to be dominant while the other two are small. For simplicity, we only consider the case where  $P_{EW}$  is fixed as the SM value.

### A. $W$ -exchange diagram $E$

It has been argued that sizable  $E$  with constructive (destructive) interference with  $C(T)$  can help to understand the large value of  $\mathcal{B}(B \rightarrow T)$  obtained when  $E$  is absent [18, 19, 20]. Since the main contribution to  $\mathcal{B}(B \rightarrow T)$  is from  $T + E$  while it is  $C - E$  for  $B \rightarrow \bar{T}$  mode. To illustrate how  $E$  improves the consistency with the  $B \rightarrow T$  data with a small  $\mathcal{B}(B \rightarrow T)$  we sketch the tree and color-suppressed tree to be

$$\mathcal{B}(B \rightarrow T) = 0.9; \quad \mathcal{B}(B \rightarrow \bar{T}) = 0.3; \quad \text{and} \quad \phi_c = 0; \quad (42)$$

respectively. The QCD penguin is fixed at  $\mathcal{B}(B \rightarrow T) = 0.1$ ,  $P = 0.5$  and  $P_{EW}$  is fixed at its SM value. In this case, the dependence of  $R_{00}$  and  $R_+$  with  $E$  and its strong phase  $\phi_c$  is plotted in Fig.7

As shown in the figure, for a small ratio of  $\mathcal{B}(B \rightarrow T) = 0.3$ , the data require a large  $\mathcal{B}(B \rightarrow T) = 0.3 - 0.5$  with a large strong phase of  $\phi_c = 2.0$ . However, The origin of large  $E$  is still a challenge for theory.

Assuming  $E$  is dominant, we find a big value from a fit to the data

$$\mathcal{B}(B \rightarrow T) = 0.46^{+0.26}_{-0.31}; \quad \phi_c = 2.36^{+0.17}_{-0.23}; \quad (43)$$

The whole fit result is given in the second column (B) of Tab.IV. The  $\chi^2_{\text{min}}/\text{d.o.f}$  is 13.2/10. Note that although  $\mathcal{B}(B \rightarrow T)$  is reduced to 0.28, the relative strong phase  $\phi_c$  is found to be large  $\phi_c = 2.1^{+0.83}_{-0.72}$  in contradiction with factorization based estimates. Thus only introducing a large  $W$ -exchange diagram will not be enough to coincide with factorization results.

An alternative way to reduce  $C(T)$  is to make  $P_{tu}$  significantly different than  $P$  or  $P_{tc}$ . This is less likely as  $P_{tu}$  is greatly suppressed relative to  $P_t$  by small  $u$ -quark mass in Wilson coefficient. The important FSI process such as charming penguin only affects  $P_{tc}$ . A fit taking  $P_{tu}$  and  $P_{tc}$  as independent parameters shows that the best fitted  $P_{tc}$  is close to the factorization estimate of  $P$  while  $P_{tu}$  is large and compatible with  $T$  in size [41], which is quite unreasonable.

As it was mentioned previously, an enhanced  $E$  has no effect in  $\bar{K}$  modes, thus can not solve the  $\bar{K}$  puzzle and explain the obtained large  $C(T) = 0$ . The best fitted branching ratios in  $\bar{K}$  still exhibit the puzzling patterns.

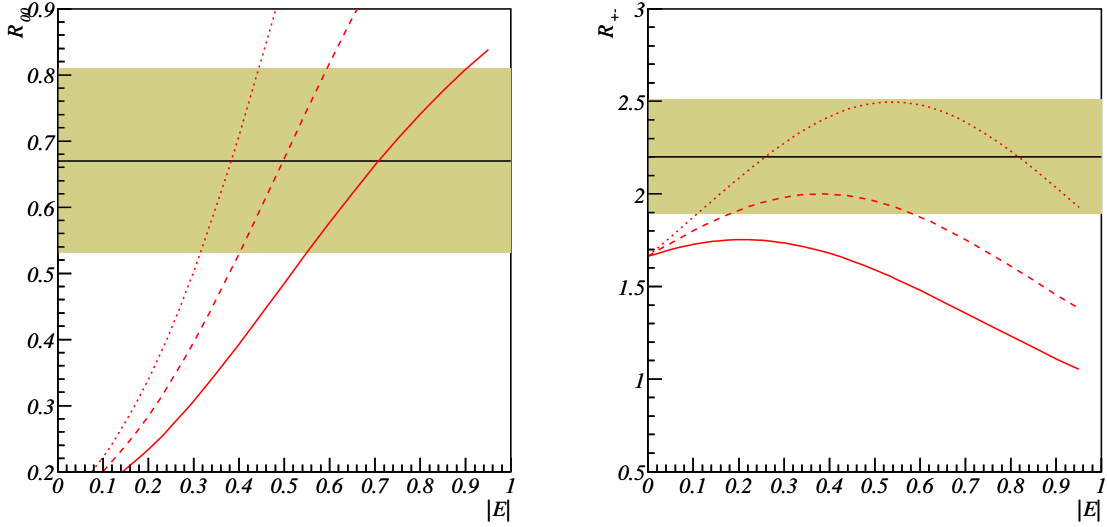


FIG. 7:  $R_{00}$  and  $R_+$  as functions of  $E$  with different values of  $\epsilon_E$ . The three curves correspond to  $\epsilon_E = 1.8$  (solid),  $2.0$  (dashed),  $2.2$  (dotted). The shadowed bands are the experimentally allowed ranges.

### B. Annihilation diagram A

The annihilation diagram A appears in  $\overline{K}^0$  and  $^0K$  modes. The current data indicate that both of them are large in comparison with  $^+K$  mode, which is characterized by the suppression of  $R_2$  and  $R$ . This may imply a sizable A in these modes as discussed in the previous sections. In Fig.8 the two ratios are given as functions of  $A$  and  $A_A$ . The other parameters are fixed at the SM best fit value in Tab.(II).

One sees from the figure that the two ratios have a similar behavior under the changing of  $A$  and  $A_A$ . For  $A$  ranges between  $0.3 \sim 0.8$ , both ratios decrease with  $A$  growing. For  $A_A = 0.5 \sim 0.8$  the curves fall down to the experimentally allowed ranges at  $A_A > 2.0$ . Since both ratios contain the same term  $A + P$ , they have similar dependences on  $A$  and  $A_A$ . This will lead to a cancellation for the ratio of the ratios:  $R/R_2 = 2B r(^0K) = B r(K^0)$  should be very close to unity, which agrees with the data well.

Assuming A is dominant over other subleading diagrams and using the scenario A for SU(3) breaking, we find

$$A_j = 0.23^{+0.12}_{-0.09}; \quad A_A = 2.77^{+0.28}_{-0.35}; \quad (44)$$

with  $\frac{2}{m_{in}} = \text{diff} = 13.8 = 10$ . The whole fitting results are listed in column (D) of Tab.IV. One sees that the best fitted value of  $A$  is moderate, which helps to reduce  $R$  and  $R_2$  but is not large enough to reproduce the central values of the two ratios. Note that even this value of  $A_j = 0.2$  is still much larger than that from factorization estimation which is suppressed by a factor of  $f_B = m_B$ .

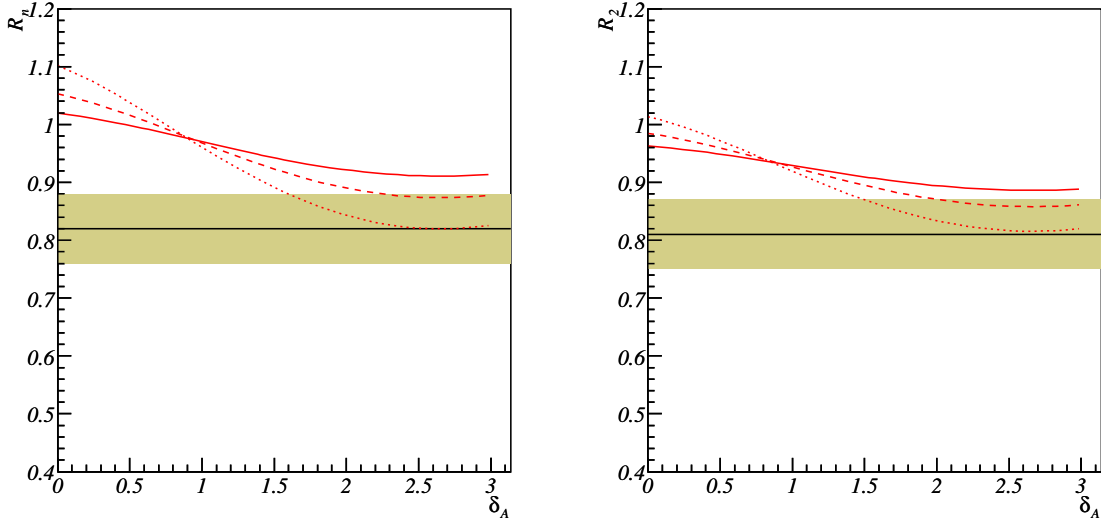


FIG. 8:  $R$  and  $R_2$  as function of  $\delta_A$  with different values of  $A$ . The three curves correspond to  $A = 0.3$  (solid),  $0.5$  (dashed),  $0.8$  (dotted). The shadowed bands are the experimentally allowed ranges.

### C. Penguin annihilation diagram $P_A$

In  $\eta$  modes, the penguin induced annihilation diagram  $P_A$  contributes to only low isospinal states ( $I = 0$ ) and it always comes together with QCD penguin  $P$  in  $\eta$  modes. Although  $P_A$  is often neglected in the literature, its effects are however effectively absorbed into QCD penguin in  $\eta$  modes. Thus the QCD penguin extracted from  $\eta$  modes are effectively  $P' = P + P_A$ . In general  $P_A$  acquires a strong phase different than that of  $P$ , namely the strong phase of  $P'$  and  $P$  are different. Since there is no SU(3) counter part  $P_A^0$  appearing in  $K$  modes,  $P^0$  still have the same strong phase as that of  $P$  in SU(3) symmetry. This introduces an effective SU(3) breaking in strong phase between  $P'$  extracted from  $\eta$  modes and  $P^0$  from  $K$ . A fit to the current data gives the following values

$$P_A = 0.035^{+0.026}_{-0.015}; \quad P_A = 2.26 \pm 0.48: \quad (45)$$

Thus its size is compatible with that of electro-weak penguin. The  $\frac{2}{m_{in}} = \text{dof}$  is found to be  $14.3/10$ . The best fitted other parameters can be found in the column (C) of Tab.IV. The best fitted value corresponds to  $P' = 0.093$  and  $P' = 0.85$ , which corresponds to a strong phase shift of

$$P = \frac{0}{P} \quad P' = 0.38: \quad (46)$$

This is in a good agreement with the previous analyses in Refs.[2, 33].

## VI. IMPLICATIONS FOR $KK$ MODES

The  $KK$  modes are much more sensitive to the subleading diagrams  $E$ ,  $A$  and  $P_A$ . The  $K^0 K^0$  mode is dominated by QCD penguin as discussed in section III. The decay amplitudes

	A	B	C	D
$\mathcal{F} j$	0:51 0:027	0:94 <sup>+0:31</sup> <sub>0:24</sub>	0:53 0:026	0:51 0:027
$\mathcal{C} j$	0:47 0:048	0:26 <sup>+0:2</sup> <sub>0:11</sub>	0:48 <sup>+0:1</sup> <sub>0:046</sub>	0:48 0:044
$c$	0:97 <sup>+0:28</sup> <sub>0:22</sub>	2:1 <sup>+0:83</sup> <sub>0:72</sub>	1:1 <sup>+0:2</sup> <sub>0:55</sub>	1:1 <sup>+0:2</sup> <sub>0:18</sub>
$\mathcal{P} j$	0:094 <sup>+0:0018</sup> <sub>0:0021</sub>	0:097 0:0022	0:094 0:0015	0:093 0:0015
$P$	0:41 0:14	0:26 <sup>+0:087</sup> <sub>0:13</sub>	0:47 <sup>+0:093</sup> <sub>0:11</sub>	0:54 <sup>+0:1</sup> <sub>0:13</sub>
$\mathcal{P}_{EW} j$	0:03 <sup>+0:019</sup> <sub>0:013</sub>	0:011 0:0011	0:011 0:0011	0:011 0:0011
$P_{EW}$	0:52 <sup>+0:31</sup> <sub>0:71</sub>	0:28 <sup>+0:14</sup> <sub>0:16</sub>	0:54 <sup>+0:11</sup> <sub>0:25</sub>	0:53 0:11
$P_{EW}^C$	0:025 <sup>+0:018</sup> <sub>0:02</sub>	0 ( x )	0 ( x )	0 ( x )
$P_{EW}^C$	2:24 <sup>+0:21</sup> <sub>0:61</sub>	0 ( x )	0 ( x )	0 ( x )
$\mathcal{E} j$	0 ( x )	0:46 <sup>+0:26</sup> <sub>0:31</sub>	0 ( x )	0 ( x )
$E$	0 ( x )	2:86 <sup>+0:17</sup> <sub>0:23</sub>	0 ( x )	0 ( x )
$\mathcal{P}_A j$	0 ( x )	0 ( x )	0:035 <sup>+0:026</sup> <sub>0:15</sub>	0 ( x )
$P_A$	0 ( x )	0 ( x )	2:26 0:48	0 ( x )
$\mathcal{A} j$	0 ( x )	0 ( x )	0 ( x )	0:23 <sup>+0:12</sup> <sub>0:087</sub>
$A$	0 ( x )	0 ( x )	0 ( x )	2:77 <sup>+0:28</sup> <sub>0:35</sub>
$2_{m \text{ in}} = \text{dof}$	11.3/10	13.2/10	14.3/10	0:93 <sup>+0:13</sup> <sub>0:16</sub>
				0:93 <sup>+0:12</sup> <sub>0:15</sub>

TABLE IV: Global fits to  $B \rightarrow K^+ K^-$ ,  $B \rightarrow K^+ K^0$  and  $B \rightarrow K^0 K^0$  data with subleading diagrams. The four columns corresponds to the four cases in each of them one subleading diagram is set to be free parameters

of the other two modes read

$$\begin{aligned}
A(K^+ K^-) &= [u(E^0, P_A^0), cP_A^0]; \\
A(K^+ K^0) &= u(P^0 + \frac{1}{3}P_{EW}^C + A^0), c(P^0 - \frac{1}{3}P_{EW}^C):
\end{aligned} \tag{47}$$

The  $K^+ K^-$  modes depend only on the subleading diagrams  $E$  and  $P_A$ . Thus it provides an ideal avenue to explore their effects. From the current upper bound of  $\text{Br}(K^+ K^-) = 1.8 [28]$ , and the SU(3) relation of scenario A, the exchanging diagram  $E$  receives a constraint of

$$\mathcal{E} j \leq 0.3; \tag{48}$$

which limits its contribution to  $B \rightarrow K^+ K^-$  modes to be moderate as the best fit to  $B \rightarrow K^+ K^-$  modes require an  $\mathcal{E} j \leq 0.48$  in Eq.(43). It is expected that stronger constraint on  $E$  will be found with more precise data in the near future.

The direct CP violations for  $K^+ K^-$  and  $K^+ K^0$  reads

$$\begin{aligned}
a_{CP}(K^+ K^-) &= \frac{2j_u c_j P_A^0 E^0 j \sin \delta \sin \delta}{j_u j^2 (\mathcal{E}^0 j^2 + P_A^0 j^2 - 2P_A^0 E^0 j \cos \delta) + j_c j^2 P_A^0 j^2 + 2j_u c_j P_A^0 j \cos \delta (\mathcal{E}^0 j \cos \delta - P_A^0 j)}
\end{aligned} \tag{49}$$

and

$$a_{CP}(K \rightarrow K^0) = \frac{2j_u^s j_c^s P^0 A^0 j \sin \delta}{j_u^s (P_A^0 + P^0) - 2P^0 P^0 j \cos \delta + j_c^s P^0 j + 2j_u^s j_c^s P^0 j \cos \delta (P^0 j \cos \delta - P^0 j)} \quad (50)$$

where  $j_u^s = P_A^0 + E^0$  and  $j_c^s = P^0 + A^0$ . In the expression of  $a_{CP}(K \rightarrow K^0)$  the color suppressed electroweak penguin are neglected. A nonzero  $a_{CP}(K \rightarrow K^0)$  will definitely indicate both nonzero  $E$  and  $P_A$ . In spite of the small branching ratio, in the case that  $E$  and  $P_A$  are compatible in size, and the strong phase difference is large, then the direct CP violation could be significant.

Unlike in the  $K$  modes where  $A$  is suppressed by a factor  $j_u^s = j_c^s = O(\lambda^2)$ , in  $K \rightarrow K^0$  mode, it is not suppressed. Thus it is promising to probe  $A$  in  $K \rightarrow K^0$  mode. A sizable annihilation diagram  $A$  will show up either through the difference between  $Br(K \rightarrow K^0)$  and  $Br(K \rightarrow K^0)$  or through the nonzero direct CP violation i.e.  $a_{CP}(K \rightarrow K^0) \neq 0$ .

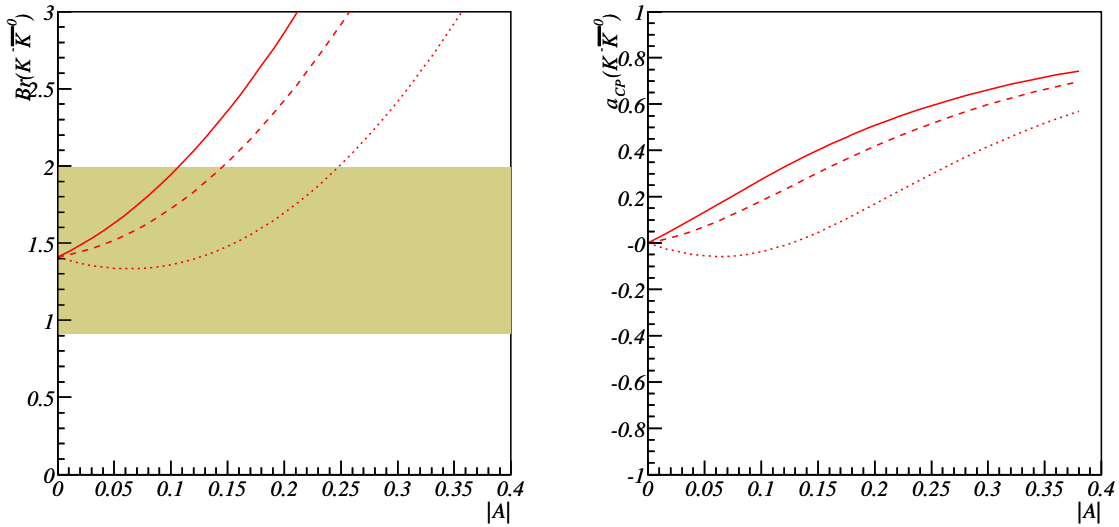


FIG. 9: Branching ratio and direct CP violation of  $K \rightarrow K^0$  as functions of  $A$  with different values of  $P_A$ . The three curves correspond to  $P_A = 0$  (solid), 2.5 (dashed), 3.0 (dotted) respectively. The shadowed band is the experimentally allowed range. Other parameters are fixed at their best fitted value in SM (according to column A of Tab.II). The SU(3) breaking effects are taken into account according to scenario A.

In Fig.9, the decay rate and direct CP violation of  $K \rightarrow K^0$  mode are plotted as function of  $A$ . In the numerical calculations, the value of  $A$  and  $P^0$  is calculated from the best fitted value of  $P$  according to scenario A. For  $P_A$  in the range 0 - 2.5, both decay rate and direct CP violation increase with  $A$  increasing. One sees from the figure that for  $P_A = 0.15 - 0.2$  and  $P_A = 2.5 - 3.0$ ,  $a_{CP}(K \rightarrow K^0)$  can reach 0.2 - 0.4 with the branching ratio in agreement with the current data. Thus with significantly large subleading diagrams, it is promising to observe large direct CP violation in this decay mode.

## V II. S U M M A R Y

In sum m ary, we have system atically studied charm less B decays  $B \rightarrow \pi^0 K^0$  and  $B \rightarrow \pi^0 K^0$ , following a strategy that making independent analysis for  $\pi^0 K^0$ ,  $K^0 K^0$  modes individually as the first step and then connecting them through various SU(3) relations. The separated analysis allowed us to clarify the origins of the inconsistency or puzzles revealed by the current data. Independent analysis on  $\pi^0 K^0$  and  $K^0 K^0$  modes both favor large ratio of  $C=T$  and  $C^0=T^0$  with large strong phases, which suggests that they are more likely to originate from long distance strong interactions rather than large non-factorizable exchange diagrams E. The sizes of QCD penguin diagrams in  $\pi^0 K^0$ ,  $K^0 K^0$  are independently extracted and were found to follow a pattern of SU(3) breaking in a good agreement with factorization estimation  $P^0=P^+$ ,  $P^0=P^0$ ,  $f_K=f$ . Global fits to these modes have been carried out under various scenarios of SU(3) relations. All the results show good determinations of weak phase  $\alpha$  in consistency with the Standard Model (SM) and prefer a large electroweak penguin ( $P_{EW}$ ) relative to  $T+C$  with a large strong phase. Within the SM, it may require an enhancement of color suppressed electro-weak penguin ( $P_{EW}^C$ ) with destructive interference to  $P_{EW}$ . The possibility of the presence of new physics effects can not be excluded. We have also investigated the possibility of sizable contributions from nonfactorizable diagrams such as E, A and  $P_A$ . Their sizes could be significantly larger than the expected ones. The typical sizes of  $P_j$  could reach to  $P_j \approx 0.3$  as required by the  $\pi^0 K^0$  and  $K^0 K^0$  data,  $P_A$  could reach to  $P_A \approx 0.2$  while  $P_A$  has a typical value of  $P_A \approx 0.03$ . The sizable subleading diagrams may change significantly the predictions for the yet to be seen  $K^+ K^0$  and  $K^+ K^0$  modes. The CP violation in  $K^+ K^0$  modes could reach  $a_{CP} \approx 0.2 \sim 0.4$  for a large value of  $A$  and  $A_A$  in the range of  $P_j = 0.15 \sim 0.2$  and  $A_A = 2.5 \sim 2.5$ . It would be encouraging to expand the investigation of subleading diagrams to decay modes involving  $\pi^0$  and  $0$  final states. Although these decay modes receive significant contributions from additional favor singlet penguin diagrams [59, 60, 61, 62] or nonstandard contributions through cc[63, 64] or QCD anomaly [65, 66], as more data points are involved, stronger constraints on the subleading diagrams will be expected. Thus it will enable us to test the SM using the full diagrammatic decomposition.

Acknowledgments

YLW is supported in part by the key project of NSFC and Chinese Academy of Sciences. YFZ is grateful to S. Sar for reading the manuscript and useful comments.

- 
- [1] K Abe, et al (Belle) Phys.Rev.D 68 012001 (2003). B Aubert, et al(Babar), hep-ex/0407057. Z Ligeti, talk at ICHEP04,Beijing,August 16-22 (2004),hep-ph/0408267. M. Giorgi, talk at ICHEP04, hep-ex/0408113, Y. Sakai, talk at ICHEP04, hep-ex/0410006.
  - [2] Y.-L.Wu and Y.-F.Zhou, Phys. Rev. D 71, 021701 (2005), hep-ph/0409221.
  - [3] Y.-Y.Keum, H.-n.Li, and A. I. Sanda, Phys. Lett. B 504, 6 (2001), hep-ph/0004004.
  - [4] Y. Y. Keum and A. I. Sanda, Phys. Rev. D 67, 054009 (2003), hep-ph/0209014.
  - [5] A. Ali and C. Greub, Phys. Rev. D 57, 2996 (1998), hep-ph/9707251.
  - [6] A. Ali, G. Kramer, and C.-D. Lu, Phys. Rev. D 58, 094009 (1998), hep-ph/9804363.

- [7] M .Beneke and M .Neubert (2003), [hep-ph/0308039](#).
- [8] M .Beneke, G .Buchalla, M .Neubert, and C .T .Sachrajda, *Phys. Rev. Lett.* 83, 1914 (1999), [hep-ph/9905312](#).
- [9] M .Beneke, G .Buchalla, M .Neubert, and C .T .Sachrajda, *Nucl. Phys. B* 591, 313 (2000), [hep-ph/0006124](#).
- [10] M .Beneke, G .Buchalla, M .Neubert, and C .T .Sachrajda, *Nucl. Phys. B* 606, 245 (2001), [hep-ph/0104110](#).
- [11] S .Barshay, G .Kreyerho , and L .M .Sehgal, *Phys. Lett. B* 595, 318 (2004), [hep-ph/0405012](#).
- [12] X .G .He and B .H .J .M cK ellar (2004), [hep-ph/0410098](#).
- [13] Y .Y .Chang and H .n .Li (2004), [hep-ph/0410005](#).
- [14] H .Y .Cheng, C .K .Chua, and A .Soni (2004), [hep-ph/0409317](#).
- [15] T .Carnuthers and B .H .J .M cK ellar (2004), [hep-ph/0412202](#).
- [16] A .A li, E .Lunghi, and A .Y .Parkhom enko, *Eur. Phys. J. C* 36, 183 (2004), [hep-ph/0403275](#).
- [17] A .Y .Parkhom enko (2004), [hep-ph/0411061](#).
- [18] A .J .Buras, R .F leischer, S .Recksiegel, and F .Schwab, *Phys. Rev. Lett.* 92, 101804 (2004), [hep-ph/0312259](#).
- [19] A .J .Buras, R .F leischer, S .Recksiegel, and F .Schwab (2004), [hep-ph/0402112](#).
- [20] A .J .Buras, R .F leischer, S .Recksiegel, and F .Schwab (2004), [hep-ph/0410407](#).
- [21] V .Barger, C .W .Chiang, P .Langacker, and H .S .Lee, *Phys. Lett. B* 598, 218 (2004), [hep-ph/0406126](#).
- [22] X .G .He, C .S .Li, and L .L .Yang (2004), [hep-ph/0409338](#).
- [23] D .London, J .M atias, and J .V irtto (2004), [hep-ph/0410011](#).
- [24] A .Datta et al. (2004), [hep-ph/0406192](#).
- [25] L .W olfenstein, *Phys. Rev. D* 52, 537 (1995).
- [26] M .Neubert, *Phys. Lett. B* 424, 152 (1998), [hep-ph/9712224](#).
- [27] J .M .G erard and J .W eyers, *Eur. Phys. J. C* 7, 1 (1999), [hep-ph/9711469](#).
- [28] For a summary, see: Heavy Flavor Averaging Group, <http://www.slac.stanford.edu/xorg/hfag/rare>.
- [29] M .Neubert, *JHEP* 02, 014 (1999), [hep-ph/9812396](#).
- [30] Y .G rossman, M .Neubert, and A .L .Kagan, *JHEP* 10, 029 (1999), [hep-ph/9909297](#).
- [31] M .G ronau and J .L .Rosner, *Phys. Lett. B* 572, 43 (2003), [hep-ph/0307095](#).
- [32] X .G .He, *Eur. Phys. J. C* 9, 443 (1999), [hep-ph/9810397](#).
- [33] Y .L .W u and Y .F .Zhou, *Eur. Phys. J. Direct C* 5, 014 (2003), [hep-ph/0210367](#).
- [34] Y .F .Zhou, Y .L .W u, J .N .Ng, and C .Q .G eng, *Phys. Rev. D* 63, 054011 (2001), [hep-ph/0006225](#).
- [35] T .Yoshikawa, *Phys. Rev. D* 68, 054023 (2003), [hep-ph/0306147](#).
- [36] D .Atwood and G .H iller (2003), [hep-ph/0307251](#).
- [37] S .M ishima and T .Yoshikawa, *Phys. Rev. D* 70, 094024 (2004), [hep-ph/0408090](#).
- [38] S .Nandi and A .Kundu (2004), [hep-ph/0407061](#).
- [39] X .G .He et al., *Phys. Rev. D* 64, 034002 (2001), [hep-ph/0011337](#).
- [40] C .W .Chiang, M .G ronau, Z .Luo, J .L .Rosner, and D .A .Suprun, *Phys. Rev. D* 69, 034001 (2004), [hep-ph/0307395](#).
- [41] C .W .Chiang, M .G ronau, J .L .Rosner, and D .A .Suprun (2004), [hep-ph/0404073](#).
- [42] J .Charles et al. (CKM tter Group) (2004), [hep-ph/0406184](#).
- [43] M .Ciuchini, E .Franco, G .Martinelli, and L .Silvestrini, *Nucl. Phys. B* 501, 271 (1997), [hep-ph/9703353](#).

- [44] M . C iuchini, E . Franco, G . M artinelli, M . P ierini, and L . Silvestrini, Phys. Lett. B 515, 33 (2001), hep-ph/0104126.
- [45] C . Isola, M . Ladisa, G . Nardulli, T . N . Pham , and P . Santorelli, Phys. Rev. D 64, 014029 (2001), hep-ph/0101118.
- [46] C . W . Bauer, I . Z . Rothstein, and I . W . Stewart (2004), hep-ph/0412120.
- [47] Y .-L . W u and Y .-F . Zhou, Phys. Rev. D 62, 036007 (2000), hep-ph/0002227.
- [48] S . Baek, P . Ham el, D . London, A . Datta, and D . A . Suprun (2004), hep-ph/0412086.
- [49] X .-G . He, C .-L . Hsueh, and J .-Q . Shi, Phys. Rev. Lett. 84, 18 (2000), hep-ph/9905296.
- [50] Z .-j . Xiao, K .-T . Chao, and C . S . Li, Phys. Rev. D 65, 114021 (2002), hep-ph/0204346.
- [51] Y . L . W u and L . W olfenstein, Phys. Rev. Lett. 73, 1762 (1994), hep-ph/9409421.
- [52] L . W olfenstein and Y . L . W u, Phys. Rev. Lett. 73, 2809 (1994), hep-ph/9410253.
- [53] Y . L . W u and Y . F . Zhou, Phys. Rev. D 61, 096001 (2000), hep-ph/9906313.
- [54] Y .-F . Zhou and Y .-L . W u, Mod. Phys. Lett. A 15, 185 (2000), hep-ph/0001106.
- [55] Y .-L . W u and Y .-F . Zhou, Phys. Rev. D 64, 115018 (2001), hep-ph/0104056.
- [56] Y .-L . W u and Y .-F . Zhou, Eur. Phys. J. C 36, 89 (2004), hep-ph/0403252.
- [57] Y .-L . W u, Chin. Phys. Lett. 16, 339 (1999), arX iv hep-ph/9805439.
- [58] Y .-L . W u and Y .-F . Zhou (2005), hep-ph/0501142.
- [59] M . G ronau and J . L . Rosner, Phys. Rev. D 53, 2516 (1996), hep-ph/9509325.
- [60] A . S . Dighe, M . G ronau, and J . L . Rosner, Phys. Lett. B 367, 357 (1996), hep-ph/9509428.
- [61] A . S . Dighe, M . G ronau, and J . L . Rosner, Phys. Rev. Lett. 79, 4333 (1997), hep-ph/9707521.
- [62] C .-W . Chiang and J . L . Rosner, Phys. Rev. D 65, 074035 (2002), hep-ph/0112285.
- [63] I . E . Halperin and A . Zhitnitsky, Phys. Rev. D 56, 7247 (1997), hep-ph/9704412.
- [64] I . E . Halperin and A . Zhitnitsky, Phys. Rev. Lett. 80, 438 (1998), hep-ph/9705251.
- [65] H . Fritzsch, Phys. Lett. B 415, 83 (1997), hep-ph/9708348.
- [66] H . Fritzsch and Y .-F . Zhou, Phys. Rev. D 68, 034015 (2003), hep-ph/0301038.